Spray Structures and Vaporizing Characteristics of a GDI Fuel Spray

Dong-Seok Choi
Department of Mechanical Engineering, Korea Advanced Institute of Science and Technology, 373-1, Kusong-Dong, Yusong-Ku, Taejon 305-701, Korea
Gyung-Min Choi
Department of Mechanical Engineering, Osaka University, 2-1 Yamadaoka, Suta, Osaka, 565-0871, Japan
Duck-Jool Kim*
School of Mechanical Engineering, Pusan National University, 30, Changjeon-Dong, Kumjeong-Ku, Pusan 609-735, Korea

The spray structures and distribution characteristics of liquid and vapor phases in non-evaporating and evaporating Gasoline Direct Injection (GDI) fuel sprays were investigated using Laser Induced Exciplex Fluorescence (LIEF) technique. Dopants were 2% fluorobenzene and 9% DEMA (diethyl-methyl-amine) in 89% solution of hexane by volume. In order to study internal structure of the spray, droplet size and velocity under non-evaporating condition were measured by Phase Doppler Anemometry (PDA). Liquid and vapor phases were visualized at different moments after the start of injection. Experimental results showed that the spray could be divided into two regions by the fluorescence intensity of liquid phase: cone and mixing regions. Moreover, vortex flow of vapor phase was found in the mixing region. About 5μm diameter droplets were mostly distributed in the vortex flow region. Higher concentration of vapor phase due to vaporization of these droplets was distributed in this region. Particularly, higher concentration of vapor phase and lower one were balanced within the measurement area at 2ms after the start of injection.

Key Words: GDI Engine, LIEF Technique, High-Pressure Swirl Injector, Fluorescence Intensity, PDA

1. Introduction

Attention has been drawn to the Gasoline Direct Injection (GDI) engine due to various potential advantages such as better fuel economy and the reduction of pollutant emissions. The mixing of fuel and air inside the cylinder of GDI engines permits the precise control over the amount of fuel burned and the injection timing. Fuel injection, therefore, is one of major factors achieving advantages of GDI engines. High-pressure swirl injectors have usually been adopted in GDI engines (Iwamoto et al., 1997; Zhao et al., 1999; Eichlseder et al., 2000). As a result, the spray strucures and vaporizing characteristics of GDI fuel spray become increasingly important.

Previous works on GDI fuel sprays can be classified into non-evaporating and evaporating sprays. Evers (1994) reported that a transient swirl spray could be divided into four regions: the leading edge, the cone, the trailing edge,

* Corresponding Author,
E-mail: djkim@hyowon.pusan.ac.kr
TEL: +82-051-510-2316; **FAX**: +82-051-516-9598
School of Mechanical Engineering, Pusan National University, 30, Changjeon-Dong, Kumjeong-Ku, Pusan 609-735, Korea. (Manuscript **Received** October 19, 2001; **Revised** March 27, 2002)

and the vortex cloud. Preussner et al. (1998) suggested the basic mechanisms of the interaction between droplets and air over a hollow-cone spray. Wicker et al. (1999) provided a more complete understanding of the instantaneous and transient GDI fuel spray structure and evolution by digital particle image velocimetry. Studies on the evaporating sprays have been mostly concentrated on diesel sprays. Yeh et al. (1994) performed the quantitative measurement of fuel vapor concentration by a Laser Induced Fluorescence (LIF) technique in a rapid compression machine, and also proposed a procedure to obtain both concentration and temperature of fuel vapor mixture in an evaporating transient diesel spray. Senda et al. (1997) applied a Laser Induced Exciplex Fluorescence (LIEF) technique to an impinging diesel spray, and quantitatively assessed vapor concentration by considering the quenching process of the fluorescence emission due to the mixture temperature and vapor concentration.

However, the evaporation processes of GDI fuel sprays are quite different from those of diesel sprays because they have the different spray patterns. Han et al. (1997) computed the internal structure of vaporizing pressure-swirl sprays. The computed results indicate that the fuel vapor exhibits a solid-cone distribution in the spray region while the liquid fuel keeps a hollow-cone structure. Ipp et al. (1999) experimentally investigated the spray formation and qualitatively provided distribution of liquid and vapor phases using LIEF technique. Choi et al. (2000, 2001) have also qualitatively investigated the effects of ambient temperature and pressure on a vaporizing GDI fuel spray using the same measurement technique. Thus, quantitative information on non-evaporating and evaporating GDI fuel sprays is experimentally required.

The objective of this study is to investigate the spray structures and the distribution of liquid and vapor phases quantitatively. For these purposes, the experiments were performed under two experimental conditions: non-evaporating and evaporating conditions. The former includes the measurement of droplet size and velocity by Phase Doppler Anemometry (PDA). The spray structure was quantitatively analyzed from this measurement. The latter includes the visualization through phase separation and quantitative measurement for fuel vapor concentration using LIEF technique.

2. Experimental Setup

Figure 1 shows the experimental setup used for investigating the high-pressure swirl sprays. The spray chamber was designed to analyze the behavior and structure of vaporizing sprays under high pressures and high temperatures. The possible maximum ambient temperature and pressure were 600K and 3MPa, respectively. Nitrogen was used as the ambient gas to prevent the quenching of liquid and vapor fluorescence by oxygen. In order to maintain a much more uniform ambient temperature profile within the test area of the spray, nitrogen flow passed through at the velocity of less than 0.1m/s inside the spray chamber. The spray chamber was purged with nitrogen and then evacuated to remove exciplex-forming dopants from previous measurements completely. Two different ambient temperatures of 293K and 473K under one ambient pressure of 0.1MPa were set to study non-evaporating and evaporating sprays.

The high fuel pressures required for direct fuel

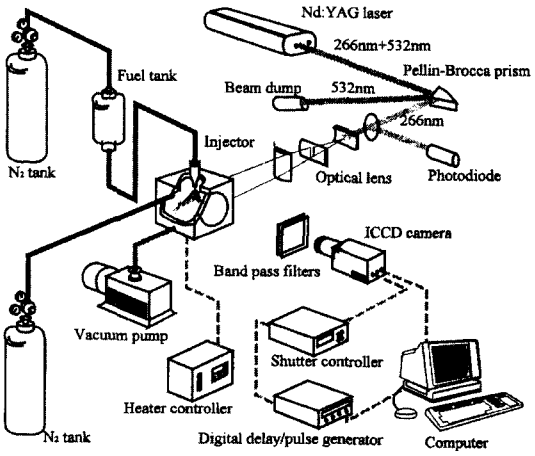

Fig. 1 Schematic diagram of experimental setup

injection were generated using a compressed nitrogen cylinder and a hydraulic accumulator in order to avoid pressure fluctuations in the fuel rail. The injector was a high-pressure swirl injector with 70° cone angle. Injection pressure was 5.1MPa as rail pressure. Injection duration and injection quantity were 2ms and 15mg, respectively, which corresponds to the medium speed and load in GDI engines.

The spray images were digitally recorded with an intensified-CCD camera that provided 640 by 480 pixel images at a resolution of 8bits. The camera system consists of a personal computer with an image grabber, a shutter controller, and a pulse generator.

The exciplex system of fluorobenzene and DEMA in a non-fluorescing base fuel of hexane was employed. The boiling points for each component are 358K, 338K, and 342K and the solution composition was 2% : 9% : 89% by volume respectively. The fourth harmonic of the Nd: YAG at 266nm with duration of 7ns and a laser energy of 50mJ/pulse was used to excite dopants from the fuel sprays. The laser beam formed a thin light sheet of 60mm high and less than 400μm thick. The filters were 300±25nm for vapor phase and 400±25nm for liquid phase. An additional WG280 sharp cut filter was used to eliminate the light at 266nm.

The PDA system consisted of a conventional Dantec fiber optic transmission unit coupled with a standard receiving unit. A 4W Argon-ion laser was used in this study. The PDA system uses a signal processor with a direct memory access interface for data transfer to a personal computer, data collection being under the control of the Sizeware software package. The green (514.5nm) laser line was used to provide the vertical droplet velocity and the phase difference for particle sizing. The focal lengths of transmitter and receiver were 400mm. A scattering angle of 30 degrees was used. The transmission and receiving optical units were mounted on a heavy-duty three-dimensional traverse, which was controlled by the Sizeware software.

Figure 2 shows the configuration of the injector tip and the spray pattern. Enlargement of the taper-type nozzle is shown on the left side of Fig. 2. To make a stratified mixture, more fuel needs to move toward spark plug in a GDI engine of wall-guided type. Thus asymmetric spray pattern has more advantages than symmetric one of a conventional injector, such as the formation of richer mixture near the spark plug. The injector used in this paper can make asymmetric spray pattern by simply cutting the nozzle tip without changing any other components (Miyajima et al, 2000). Fuel is supplied from the top of the injector and rotational momentum is given to the fuel by a swirler. Fuel flows into the orifice while the valve is being lifted. Thus fuel spray is intermittently injected from the orifice into the spray chamber. Spray axis has a slope of 5 degrees from vertical axis in a direction of counter-clock wise due to the configuration of the injector tip. Toroidal vortex appears at the both sides of the spray, which is the typical characteristic of high-pressure swirl sprays.

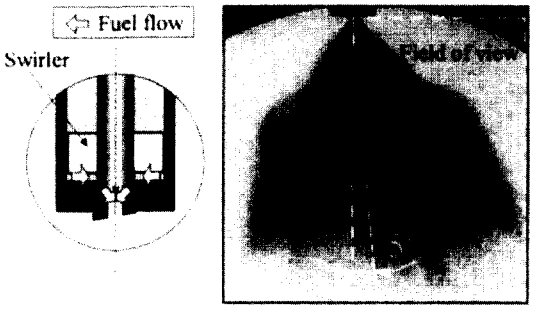

Fig. 2 Injector tip configuration and spray pattern

3. Results and Discussion

3.1 Visualization of liquid and vapor phase

Figures 3 (a), (b) and (c) show the spray evolution under non-evaporating (T_a=293K) and evaporating (T_a=473K) conditions. The visualization was performed only on the part of the image to the right of the spray axis (the side of the incoming laser sheet) to minimize errors due to the attenuation of the laser sheet by the spray. The image processing was done on a set of five images for each condition. The images were scaled with respect to laser power and camera

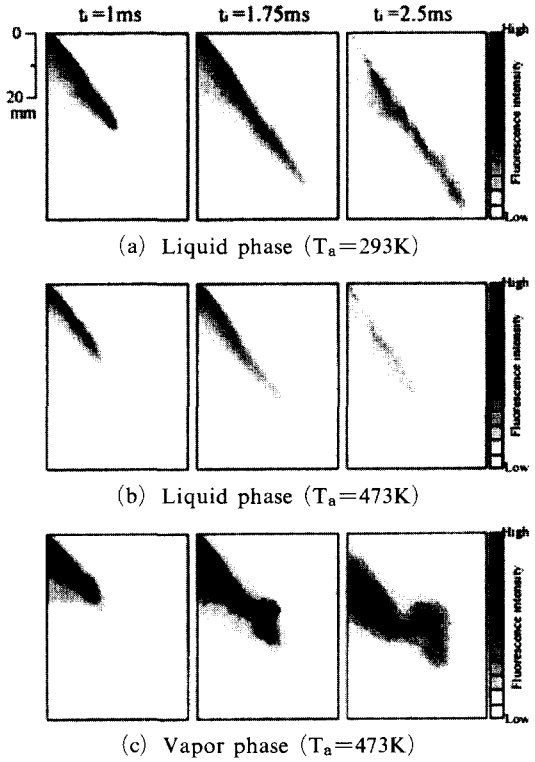

(a) Liquid phase (T_a=293K)

(b) Liquid phase (T_a=473K)

(c) Vapor phase (T_a=473K)

Fig. 3 Spray evolution for liquid and vapor phases

gain, and normalized using the measured vertical sheet profiles. When comparing liquid and vapor phases under evaporating condition, the spatial distributions of liquid phase were decreased with time after the start of injection while those of vapor phase were increased. For liquid phase, fluorescence intensity was high in the outer region of the spray. With an increase in ambient temperature, fluorescence intensity became low downstream of the spray. This indicates that droplets change into fuel vapor in that region. However, the variation of fluorescence intensity near the injector tip was not significant. This indicates that liquid phase near the injector tip is dense and the vaporization of droplets is not active. For vapor phase, high fluorescence intensity appeared in the internal spray region where the vortex structure (Han et al, 1997) was formed.

Figure 4 shows the profiles of relative fluorescence intensity for liquid phase along the 40 degrees inclined line from vertical axis at 2ms after the start of injection. Generally, swirl sprays

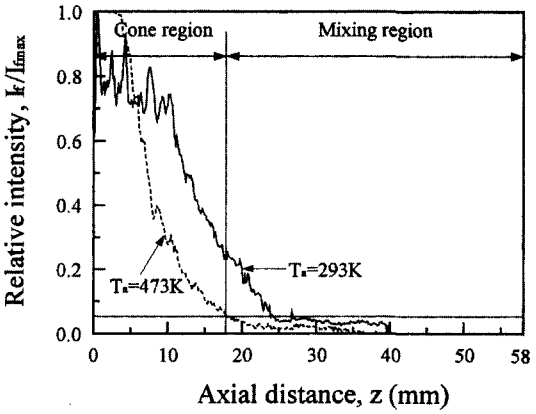

Fig. 4 Classification of cone and mixing regions by the intensity of liquid phase

could be divided into two regions. One is cone region surrounded by main spray. The other is mixing region where the spray motion creates the vortex flow of ambient gas due to mixing of droplet and ambient gas. In order to distinguish these regions, the spray angle of fully developed spray was considered 40 degrees from visualized images. The relative intensity was defined as the ratio of each fluorescence intensity on the inclined line averaged within ± 5 degrees of the spray angle to maximum fluorescence intensity. These relative intensities under non-evaporating and evaporating conditions were compared in Fig. 3. From this figure, the distance of about 18mm from the injector tip determined the range of cone region. This distance corresponds to 5% of the maximum relative intensity under evaporating condition. The rest region of the spray was defined as mixing region.

3.2 Distribution of droplet size and velocity

Figure 5 shows size distribution of droplets measured by the PDA system. Data were collected over many injections until 10,000 validated data samples had been acquired for each measurement point. After then the droplets from the start of injection to 10ms after injection were collected from validated data samples. For all measurement points, the arithmetic mean diameter is 11μm, and the SMD, which is very important for droplet vaporizing and combustion, is 23μm. This SMD

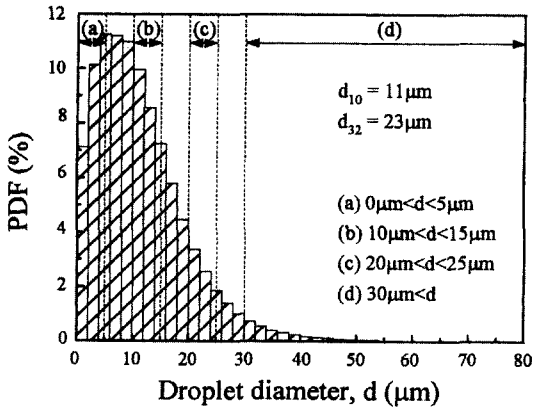

Fig. 5 Droplet size distribution

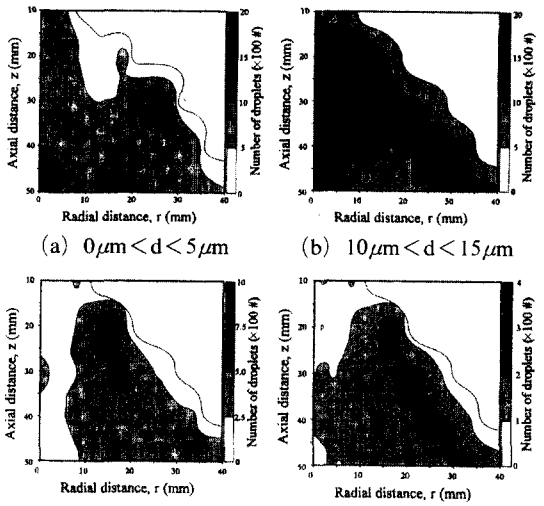

Fig. 6 Number density distribution with size-classified droplets

is an acceptable level for the spray characteristics of GDI fuel sprays (Zhao et al., 1999). To analyze the effect of droplet size on the spray structure, those droplets were again classified into four size classes as shown in Fig. 5. Small size class below 5μm diameter droplets (a) follows the airflow due to their small momentum. Medium size classes of droplets were classified into two size classes. One (b) is droplets of 10 to 15μm in diameter above Probability Density Function (PDF) of 5%. The other (c) is droplets of 20 to 25μm in diameter below PDF of 5%. Large size class above 30μm diameter droplets (d) could be predicted the main flow of the spray due to their great momentum.

Figures 6 (a), (b), (c) and (d) show the distributions of droplet number density. Diameters of size-classified droplets were averaged at each measurement point and presented in two dimensions. These two-dimensional distributions show that which size class of droplets has a significant effect on droplet vaporization. Fine droplets below 5μm in diameter (a) were distributed around the vortex region, as mentioned in Fig. 3. However, larger droplets above 30μm in diameter (d) were mostly distributed in the outer region of the spray. This indicates that larger droplets gather outside the spray due to the swirl momentum of the main spray while smaller droplets gather inside the spray due to air-entrainment. Especially, the vortex region was formed by the momentum exchange between entrained air and fine droplets with small momentum. Vapor phase follows this vortex flow. It is also expected that higher vapor concentration due to mixing with ambient gas and more active vaporization could occur in this region. This will be also verified in the next section through the quantitative distribution of vapor phase. Medium size class of droplets (b) was concentrated in the inner region of the spray. Size class of droplets (c) was slightly distributed in the outer region of the spray. Thus internal region of this GDI fuel spray was mostly filled with droplets of 10 to 15μm (upper medium size class) in diameter.

Figure 7 shows vector plots of size-classified droplets. Droplets below 5μm in diameter follow ambient gas flow because they have small momentum. For cone region, the peak velocity of these droplets appears high at the outer region of the spray and near spray axis. For mixing region, the peak velocity is near the spray axis. This indicates that ambient gas moves into the spray. Generally, the inner region of a hollow cone spray becomes dynamic vacuum state due to the momentum exchange between main spray and ambient gas (Preussner et al, 1998). This state makes ambient gas move into the spray. Thus, the inner spray region is filled with fine droplets with small

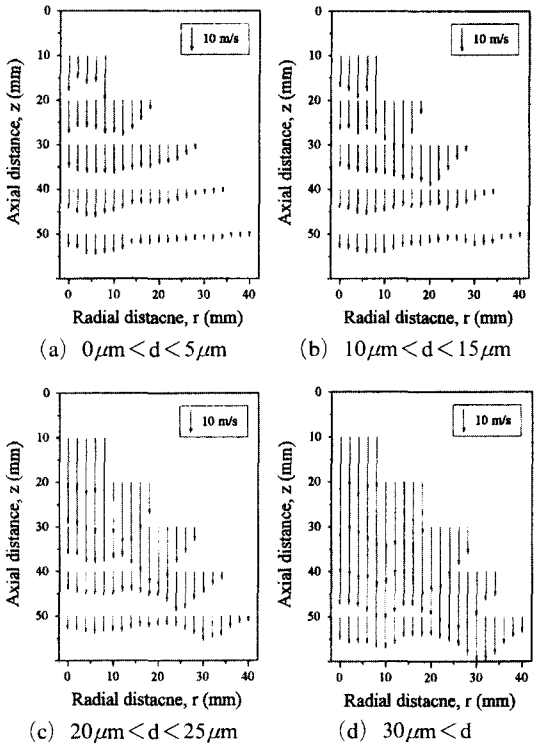

Fig. 7 Profiles of axial velocity with size-classified droplets

momentum due to this ambient gas motion. Therefore, two peak velocity in the cone region and one peak velocity in the mixing region appear due to this momentum exchange. The size class of 10 to 15μm diameter droplets with the highest droplet number density maintains the momentum of the main spray in the cone region. These droplets have high velocity distribution in the outer region of the spray due to swirl momentum of the main spray. However, they lose their momentum in the mixing region and follow ambient gas flow. On the other hand, slightly higher velocity profiles appear in the central mixing region. The size class of 20 to 25μm diameter droplets has typical velocity distribution of a hollow cone spray, namely higher velocity distribution in the outer region of the spray. The droplets above 30μm in diameter maintain the momentum of main spray in the overall spray region and have higher velocity.

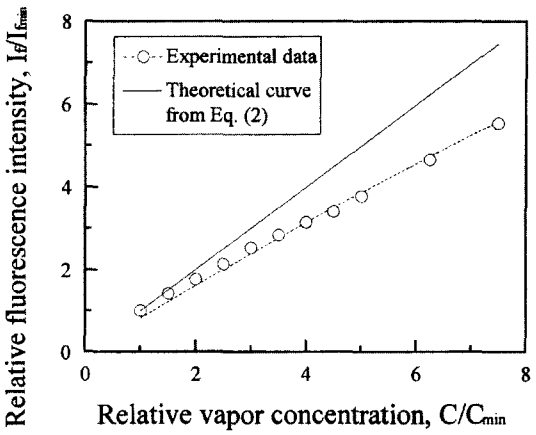

Fig. 8 Comparison between experimental result and theoretical value for vapor concentration

3.3 Quantification of vapor concentration

When the sectional area of the spray is divided into the mesh of number n with the same length L along the incident laser light sheet irection, the intensity of laser light sheet (I_i) at the i-th mesh is given by the following equation.

$$I_i = I_0 \exp\left(-\varepsilon \cdot L \cdot \sum_{i=1}^{n} C_i\right) \quad (1)$$

where I_0 : intensity of incident laser light sheet ($J/m^2 \cdot s$)

ε : molar absorption coefficient for the wavelength of incident laser light sheet ($m^3/mol \cdot m$)

L : length of mesh (m)

n : number of pixels

Fluorescence intensity at the i-th mesh (I_{fi}) is given by Eq. (2). Concentration of fluorescence material at i-th mesh can be obtained from this equation.

$$I_{fi} = A \cdot K \cdot I_0 \cdot \exp\left(-\varepsilon \cdot L \cdot \sum_{i=1}^{n} C_{i-1}\right) \cdot \{1 - \exp(-\varepsilon \cdot C_i \cdot L)\} \quad (2)$$

where A : proportional constant associated with the optical systems

K : rate coefficient for the excited transition

C_i : molar concentration of fluorescence material at the I-th mesh (mol/m^3)

Figure 8 shows the change in fluorescence in-

tensity ratio with different vapor concentration ratios at the ambient pressure of 0.1MPa and ambient temperature of 473K, where two relative ratios are normalized with the minimum intensity ($I_{f,\min}$) and minimum concentration ($C_{v,\min}$), respectively. In this figure, a solid line is the theoretical value from Eq. (2), and a dotted line represents the experimental data obtained from the calibration test. The length of mesh is 1.4×10^{-4}(m) and ε is 73.56m^3/(mol·m) for incident laser light sheet of 266nm. The difference between the experimental result and theoretical one in this figure seems to be attributed to the quenching effect of the vapor concentration. This value (K_{cq}) is obtained from Fig. 9. Thus, Eq. (2) should be transformed as follows.

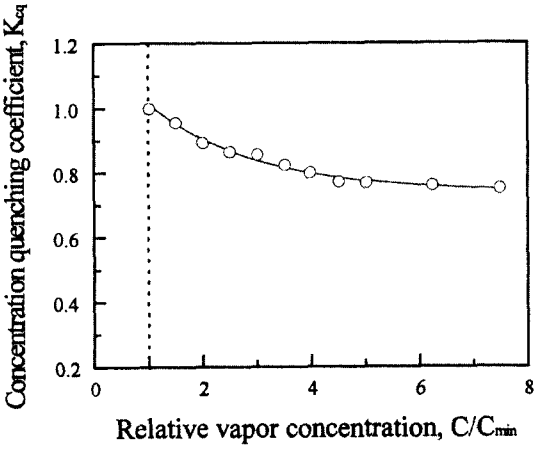

Fig. 9 Concentration quenching coefficient with different vapor concentration ratios

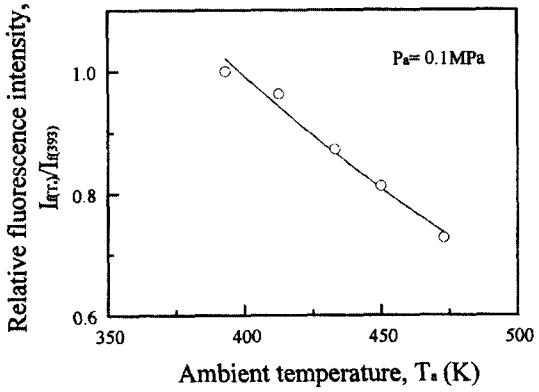

Fig. 10 Change in relative fluoreseence intensity of vapor phase with different ambient temperatures

$$I_{fi}=A\cdot K\cdot K_{cq}\cdot I_0\cdot\exp\left(-\varepsilon\cdot L\cdot\sum_{i=1}^{n}C_{i-1}\right)\cdot\{1-\exp(-\varepsilon\cdot C_i\cdot L)\} \quad (3)$$

Temperature is also one of quenching factors. In order to correct quenching effects of temperature, the relation between the relative fluorescence intensity ratio and the temperature was investigated. The result was shown in Fig. 10. Quantitative analysis scheme for vapor concentration provided by Senda et al. (1997) was used. The spray images were then converted into concentration values (mol/m^3).

3.4 Vaporizing characteristics

There are some limitations in applying the calibration results for vapor phase to the spray. In other words, absorption and scattering of laser light by liquid droplets are high when laser light passes through a dense spray. Thus, it is difficult for the calibration results to be directly applied to the spray. For this reason, the quantification region for vapor phase was determined as mixing region where there is no or little liquid phase under evaporating conditions. Figure 11 shows two-dimensional distributions of vapor concentration. The quantified images were presented

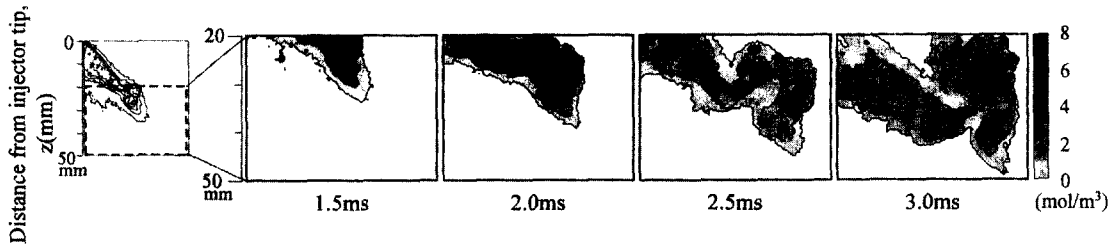

Fig. 11 Concentration distributions of vapor phase

from 1.5ms after the start of injection to 3ms. The quantified area was between 20mm and 50mm downstream of the injector tip. The vortex structure is being developed after 2ms due to the momentum exchange between swirl momentum of the spray and air entrainment explained in Fig. 7. As mentioned in Fig. 6, fine droplets below 5μm in diameter lose their momentum and follow the reverse ambient gas flow. Vapor phase also follows this gas flow and consequently the vortex structure develops. From the concentration distri -ution, higher concentration due to vaporization of many fine droplets appears at 2ms after the start of injection. In addition, the concentration fields become increasingly uniform due to mixing of droplets and ambient gas.

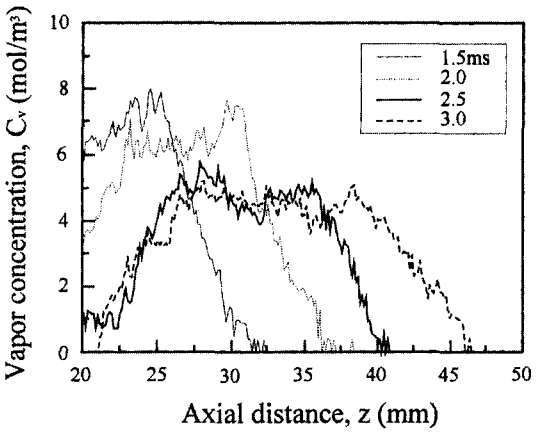

Fig. 12 Distribution of vapor concentration along the 40 degrees inclined line from vertical axis

Figures 12 and 13 show axial and radial distribution of vapor concentration for the mixing region from 1.5ms to 3ms after injection start. Figure 12 shows the distribution of vapor concentration along the 40 degrees inclined line from vertical axis. In the injection period, the concentration higher than 6mol/m^3 appears locally in the vortex region as mentioned in Fig. 6. Concentration distribution after the end of injection period becomes more uniform and wider than that in the injection period. This indicates that small-scale vortex is formed in the injection period while large-scale vortex develops from small-scale vortex after the end of injection period. Thus this large-scale vortex promotes the vaporization of fine droplets. Figure 13 shows radial distribution of vapor concentration at axial distance of 30mm below injector tip. This distance is equivalent to the length between injector tip and piston bowl at the late injection mode of GDI engines. In the injection period, most vapor phase concentrated in the spray tip region and had non-uniform concentration distribution. In the period after the end of injection, vapor phase distributed widely due to the developed vortex and the internal region of the spray was filled with the concentration above 3mol/m^3.

Figure 14 shows vaporization characteristics according to the area ratio of vapor concentration. This ratio was defined as the ratio of the

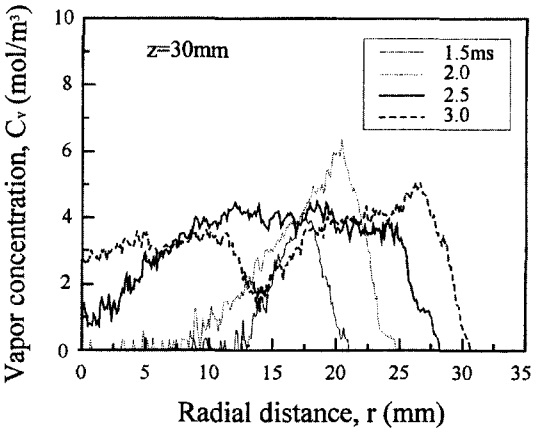

Fig. 13 Radial distribution of vapor concentraion at 30mm below injector tip

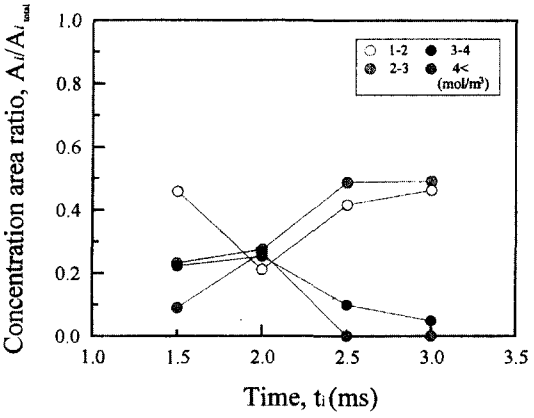

Fig. 14 Change in concentration area ratio with time after injection start

area of classified vapor concentration (A_i) to spray area within quantified area ($A_{i,total}$). Vapor concentration below 3mol/m^3 remained in the developed vortex cloud at 3ms after the end of injection. Therefore, the concentration greater than 3mol/m^3 was considered high while the concentration below 3mol/m^3 was considered low. High and low classified concentrations have similar portion at 2ms after the start of injection. This is considered as the balance time between two classified concentrations.

4. Conclusions

Distribution characteristics of liquid and vapor phases in non-evaporating and evaporating GDI fuel sprays have been investigated using LIEF technique. To analyze the spray structure, droplet size and velocity were measured by the PDA system under non-evaporating condition. The main conclusions are summarized as follows:

(1) GDI fuel spray could be divided into cone and mixing regions according to the fluorescence intensity of liquid phase.

(2) Entrained airflow accelerated axial velocity near the spray axis and formed vortex flow in the outer edge of the spray. Droplets below 15μm in diameter mostly followed this airflow.

(3) The size class of 10 to 15μm diameter droplets had higher number density than other size classes and distributed widely in the spray region.

(4) The vortex flow formed in the outer edge of the spray promoted the vaporization of droplets, as the result higher vapor concentration appeared in this region.

(5) Higher vapor concentration (above 3mol/m^3) and lower one kept the balance at time of 2ms after the start of injection.

References

Choi, D., Kim, D. and Hwang, S., 2000, "Development Behavior of Vaporizing Sprays from a High-Pressure Swirl Injector using Exciplex Fluorescence Method," *KSME International Journal*, Vol. 14, No. 10, pp. 1143~1150.

Choi, D. and Kim, D., 2001, "Vaporizing Characteristics of Spray from Two Different GDI Injectors," Tran. of the KSME, B, Vol. 25, No. 5, pp. 688~696, (in Korean).

Eichlseder, H., Baumann, E., Muller, P. and Rubber, S., 2000, "Gasoline Direct Injection-A Promising Engine Concept for Future Demands," *SAE paper*, No. 2000-01-0248.

Evers, L. W., 1994, "Characterization of the Transient Spray from a High Pressure Swirl Injector," *SAE paper*, No. 940188.

Han, Z. and Reitz, R. D., 1997, "Internal Structure of Vaporizing Pressure-Swirl Fuel Sprays," *Proc. ICLASS-97*, pp. 474~481.

Ipp, W., Wagner, V., Kr mer, H., Wensing, M., Leipertz, A., Arndt, S. and Jain, A. K., 1999, "Spray Formation of High Pressure Swirl Gasoline Injectors Investigated by Two-Dimensional Mie and LIEF Techniques," *SAE paper*, No. 1999-01-0498.

Iwamoto, Y., Noma, K., Nakayama, O., Yamauchi, T. and Ando, H., 1997, "Development of Gasoline Direct Injection Engine," *SAE paper*, No. 970541.

Miyajima, A., Okamoto, Y., Kadomukai, Y., Togashi, S. and Kashiwaya, M., 2000, "A Study on Fuel Spray Pattern Control of Fuel Injector of Gasoline Direct Injection Engines," *SAE paper*, No. 2000-01-1045.

Preussner, C., Doring, C., Fehler, S. and Kampmann, S., "GDI: Interaction Between Mixture Preparation, Combustion System and Injector Performance," *SAE paper*, No. 980498.

Senda, J., Kanda, T., Kobayashi, M., Fujimoto, H., 1997, "Quantitative Analysis of Fuel Vapor Concentration in Diesel Spray by Exciplex Fluorescence Method," *SAE paper*, No. 970796.

Wicker, R. B., Loya, H. I., Hutchison, P. A. and Sakakibara, J., 1999, "SIDI Fuel Spray Structure Investigation Using Flow Visualization and Digital Particle Image Velocimetry," *SAE paper*, No. 1999-01-3535.

Yeh, C., Kamimoto, T., Kosaka, H. and Kobori, S., 1994, "Quantitative Measurement of 2-D Fuel Vapor Concentration in a Transient

Spray via Laser-Induced Fluorescence Technique," *SAE paper*, No. 941953.

Zhao, F., Lai, M. and Harrington, D. L., 1999, "Automotive Spark-Ignited Direct-Injection Gasoline Engines," *Progress in Energy and Combustion Science*, Vol. 25, pp. 437~562.